Supplementary Materials

Liquid crystal polyarylate tailored functionalized boron nitride alignment for constructing high thermal conductivity composites

Qingbao Guan[1], Jian Liu[1], Haiyang Zhang[1], Jingyi Lu[2,*], Ping Liu[3], Xiaolan Qiao[1,*], Zhengwei You[1,4], Meifang Zhu[1,*]

[1]State Key Laboratory of Advanced Fiber Materials, College of Materials Science and Engineering, Research Base of Textile Materials for Flexible Electronics and Biomedical Applications (China Textile Engineering Society), Shanghai Engineering Research Center of Nano-Biomaterials and Regenerative Medicine, Donghua University, Shanghai 201620, China.
[2]Key Laboratory of Smart Manufacturing in Energy Chemical Process, Ministry of Education, East China University of Science and Technology, Shanghai 200237, China.
[3]NETZSCH Scientific Instruments (Shanghai) Co. Ltd., Shanghai 200131, China.
[4]Shandong Inov Polyurethane Co., Ltd., Zibo 255086, Shandong, China.

[*]**Correspondence to:** Prof. Xiaolan Qiao, Prof. Meifang Zhu, State Key Laboratory of Advanced Fiber Materials, College of Materials Science and Engineering, Research Base of Textile Materials for Flexible Electronics and Biomedical Applications (China Textile Engineering Society), Shanghai Engineering Research Center of Nano-Biomaterials and Regenerative Medicine, Donghua University, Shanghai 201620, China. E-mail: xlqiao@dhu.edu.cn; zmf@dhu.edu.cn; Prof. Jingyi Lu, Key Laboratory of Smart Manufacturing in Energy Chemical Process, Ministry of Education, East China University of Science and Technology, Shanghai 200237, China. E-mail: jylu_cise@ecust.edu.cn

Content

Experimental Section: Characterizations of BN-G and LCP-BN-Gs
Supplementary Table 1. List of test instruments
Supplementary Table 2. Thermal stability parameters of pure LCP and LCP-BN-G composites with different BN-G loadings: temperature at 5% weight loss ($T_d^{5\%}$), maximum decomposition temperature (T_{dmax}), and char yield at 600 °C (*Y*c@600°C).
Supplementary Table 3. Diffraction peak intensities of (002) and (100) planes and the calculated orientation degree (φ) of BN-G in LCP-BN-G composites with different BN-G loadings.
Supplementary Table 4. Specific heat capacity and density of LCP and LCP-BN-G composites.
Supplementary Figure 1. FT-IR spectra of pure LCP and the LCP-BN-Gs composites.
Supplementary Figure 2. Characterization of pristine BN and functionalized BN-G with a magnified view of the (002) diffraction peaks
Supplementary Figure 3. TGA curves of LCP and its BN/BN-G composites.
Supplementary Figure 4. Azimuthal intensity profiles of the LCP matrix at 2θ≈20°.
Supplementary Figure 5. Dielectric properties of LCP and its BN/BN-G composites (a) dielectric constant and (b) dissipation factor.
Supplementary Figure 6. Rheological behavior curves of LCP and its BN/BN-G composites.
Supplementary Figure 7. Comparative SEM fracture surface morphologies of neat LCP, LCP-BN, and LCP-BN-G composites at different magnifications: (a) LCP, (b) LCP-BN-G-10, (c) LCP-BN-G-20, (d) LCP-BN-10, and (e) LCP-BN-20.
Supplementary Figure 8. The surface element distribution of the LCP-BN-G-20.
Supplementary Figure 9. Comparison of surface temperature variation between pure LCP and LCP-BN-G-20 substrates during 3600 s of continuous LED operation.
Supplementary Figure 10. Surface temperature variation of pure LCP and LCP-BN-G-20 substrates during ten cycles of 60 s heating and 30 s cooling.

Experimental Section

Characterizations of BN-G and LCP-BN-Gs: The chemical structures of the samples were characterized using a Nicolet 8700 Fourier transform infrared spectrometer (Thermo Scientific). For the BN and BN-G powder samples, measurements were performed using the KBr pellet method; for the LCP-BN-G composites, direct testing was carried out with an attenuated total reflection (ATR) accessory. All spectra were collected over 32 scans with a wavenumber range of 4000-500 cm^{-1}.

X-ray photoelectron spectroscopy (XPS) measurements were performed on a Thermo Scientific Escalab 250Xi spectrometer using monochromatic Al Kα radiation. The test sample was BN-G powder with a mass of 10–20 mg. The binding energy scale was calibrated by referencing the adventitious C 1s peak to 284.8 eV. All spectra were recorded at room temperature.

A Libra/209F1 TGA was used to study the thermal stability. The samples were analyzed using a heating rate of 10 °C min^{-1}. All measurements were conducted from 40°C to 600 °C under a nitrogen atmosphere.

The melt behavior of the LCP-BNs was determined by differential scanning calorimetry (DSC) using TA DSC-Q20 with a heating rate of 20 °C min^{-1}. All measurements were conducted from 30 °C to 380 °C under a nitrogen atmosphere.

Dynamic mechanical analyses (DMA) were performed with a NETZSCH DMA303. in tension mode, using thin films (20 ± 0.2) mm × (5 ± 0.2) mm × (0.5 ± 0.1) mm under a nitrogen atmosphere and at a heating rate of 5 °C min^{-1}. All experiments were performed at a frequency of 1.0 Hz.

The dielectric constant (ε') and dissipation factor ($tan\ \delta$) were recorded with a broadband dielectric impedance spectrometer. Frequency multiplexing was adjusted from 10^0 to 10^7 Hz at test temperature of 25 °C. The samples were hot pressed in to sheets, cut into wafers with a diameter of 20 mm and a thickness of less than 0.7 mm, and laminated with copper foil on both sides.

The rheological behavior of the composites were investigated using Kinexus Prime Lab+ (Netzsch, Germany) stress controlled rotational rheometer, equipped with the parallel plate geometry. The test specimens were prepared as circular discs with a diameter of 20 mm and a thickness of 1 mm. A normal force of 1 N was applied prior to testing to ensure optimal contact between the sample and the fixture. Measurements were conducted in an air atmosphere, with the temperature ramped from 50 °C to 370 °C at a heating rate of 3 °C/min. The test frequency was fixed at 1

Hz with a strain amplitude of 0.1%.

The crystal structure of the samples was analyzed using a Cu- Kα radiation source (wavelength λ = 0.154 nm). The scanning range (2θ) was set from 10° to 50°, with a step size of 0.02° and an exposure time of 0.1 s per step.

Wide-angle X-ray scattering (WAXS) measurements were performed on a Rigaku HomeLab diffractometer equipped with a Hypix-6000 high-sensitivity single-photon counting pixel detector, with an effective pixel size of 100 μm×100 μm. The measurements were carried out using Cu Kα radiation (λ=1.5405 Å) as the X-ray source. The sample-to-detector distance (SDD) was precisely calibrated using standard silicon powder (Si) as the reference. During the experiments, the samples with dimensions of 7 mm × 7 mm and a thickness of 0.6 mm were vertically mounted in the X-ray beam path, and the two-dimensional wide-angle X-ray scattering (2D-WAXS) patterns were recorded by the detector and exported. For data processing, the obtained 2D diffraction patterns were imported into the Fit2D software (European Synchrotron Radiation Facility, ESRF) for subsequent analysis. To quantitatively evaluate the influence of the shear flow field during melt processing on the orientation degree of the liquid crystal polyarylate (LCP) matrix molecular chains, the characteristic diffraction peak of the LCP matrix at 2θ≈20° was selected. The azimuthal scan (Azimuthal angle, ϕ) was performed to integrate the diffraction intensity of this peak. The full width at half maximum (*FWHM*) of the azimuthal diffraction peak was extracted by fitting the data with a Lorentzian function. The relative orientation degree (Π) of the LCP matrix molecular chains was subsequently calculated according to the empirical formula:

$$\Pi = \frac{180^\circ - FWHM}{180^\circ} \times 100\%$$

A high-resolution JEOL scanning electron microscope (SEM) and energy dispersive spectroscopy (EDS) operating at 5 kV was used to investigate the morphology of the fracture surfaces of the films.

The heat dissipation performance of LCP films was evaluated using a laboratory- customized LED cooling system. An LED lamp with a rated power of 20 W was employed. A Fotric 325C infrared thermal imager was used to monitor the LED surface temperature during operation.

Thermal conductivity is a key parameter for evaluating the heat transfer capability of a material. It is calculated using the following formula:

$$K=\alpha\times C_P\times\rho$$

Where K is the thermal conductivity, α is the thermal diffusivity, Cp is the specific heat capacity, and ρ is the density. The measurement methods for each parameter are described below.

Thermal diffusivity was measured using a NETZSCH LFA 467 laser flash analyzer (transient method, Germany). Composite films were cut into circular discs with diameters of 12.7 mm or 25 mm and a thickness of 0.5 mm. Before testing, both surfaces of the samples were uniformly coated with graphite. Thermal diffusivity was measured in both the in-plane and through-plane directions.

Specific heat capacity was determined using the sapphire reference method via differential scanning calorimetry (DSC). In this method, the sample and a sapphire standard with known specific heat capacity are tested under identical conditions. The specific heat of the sample is calculated using the following equation:

$$C_2=\frac{(Y_2-Y_1)\times m_1}{(Y_1-Y_0)\times m_2}\times C_1$$

Where C_1 is the specific heat capacity of sapphire, C_2 is the specific heat capacity of the sample, m_1 and m_2 are the masses of sapphire and the sample, respectively, and Y_0, Y_1, and Y_2 represent the DSC heat flow values of the baseline, sapphire, and sample at a given temperature.

The testing procedure was as follows: cooling from 40 °C to -20 °C at 20 °C·min^{-1}, holding at -20 °C for 10 min, and then heating to 100 °C at 5 °C·min^{-1}.

Density was determined based on Archimedes' principle using the liquid immersion method. The procedure was as follows: first, the mass of the sample together with a thin suspension wire was measured in air; then, the sample was fully immersed in a solvent of known density, and the apparent mass was measured in the solvent. Density was calculated using the formula:

$$\rho=\frac{w_1}{w_1-w_0}\times\rho_{solvent}$$

Where w_1 is the total mass of the sample and suspension wire in air, w_0 is the total mass of the sample and wire in the solvent, and $\rho_{solvent}$ is the density of the solvent at the test temperature.

Supplementary Table 1. List of test instruments

Instrument	Model	Manufacturer
Fourier Transform Infrared Spectrometer (FT-IR)	Nicolet 8700	Thermo Fisher Scientific
Differential Scanning Calorimeter (DSC)	Q20	TA Instruments
Differential Scanning Calorimeter (DSC)	204F1	Netzsch
In-situ X-ray Diffractometer (XRD)	D2 phaser	Bruker
Wide-angle X-ray Scattering Diffractometer (2D WAXD)	HomeLab	Rigaku
X-ray Photoelectron Spectrometer (XPS)	Escalab 250Xi	Thermo Scientific
Thermogravimetric Analyzer (TGA)	Libra/209F1	Netzsch
Dynamic Mechanical Analyzer (DMA)	DMA303	Netzsch
Rotational Rheometer	Kinexus Prime Lab+	Netzsch
Rotational Rheometer	MCR702	Anton Paar
Scanning Electron Microscope (SEM) with EDS	JSM-7500F	JEOL Ltd.

Instrument	Model	Manufacturer
Broadband Dielectric Impedance Spectrometer	Concept 40	Novocontrol
Micro Compounder	CTS-15	Shanghai Changkai Electromechanical Technology Co., Ltd.
Infrared Thermal Imager	325C	Fotric
Laser Flash Analyzer (LFA)	LFA467	Netzsch

Supplementary Table 2. Thermal stability parameters of pure LCP and LCP-BN-G composites with different BN-G loadings: temperature at 5% weight loss ($T_d^{5\%}$), maximum decomposition temperature (T_{dmax}), and char yield at 600 °C (*Y*c@600 °C)

Sample	$T_d^{5\%}$ (°C)	T_{dmax} (°C)	*Y*c@600 °C (%)
LCP	464	489	54.03
LCP-BN-G-5	458	485	53.90
LCP-BN-G-10	447	487	54.72
LCP-BN-G-15	446	489	56.49
LCP-BN-G-20	430	491	58.27

Supplementary Table 3. Diffraction peak intensities of (002) and (100) planes and the calculated orientation degree (φ) of BN-G in LCP-BN-G composites with different BN-G loadings

Sample	I_{002}	I_{100}	φ
LCP-BN-G-5	804	157	83.66
LCP-BN-G-10	1124	174	86.59
LCP-BN-G-15	1923	240	88.90
LCP-BN-G-20	1359	205	86.89

Supplementary Table 4. Specific heat capacity and density of LCP and LCP-BN-G composites

Sample	Specific heat capacity ($J \cdot g^{-1} \cdot K^{-1}$)	Density (g/cm^3)
LCP	0.98351	1.223
LCP-BN-G-5	0.84802	1.209
LCP-BN-G-10	1.15075	1.386
LCP-BN-G-15	0.98456	1.445
LCP-BN-G-20	0.94599	1.551

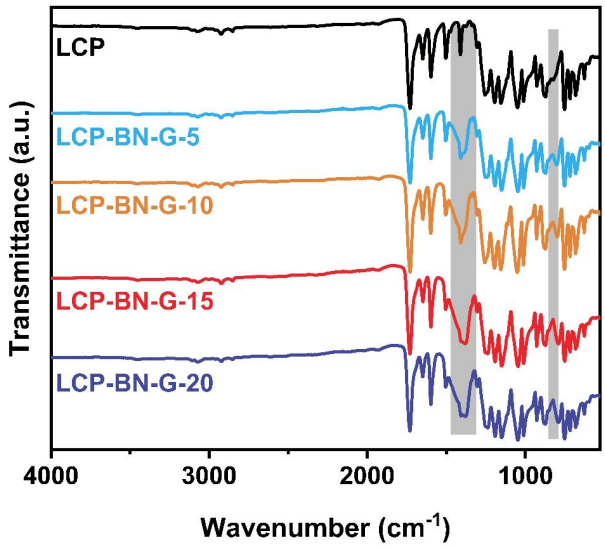

Supplementary Figure 1. FT-IR spectra of pure LCP and the LCP-BN-Gs composites.

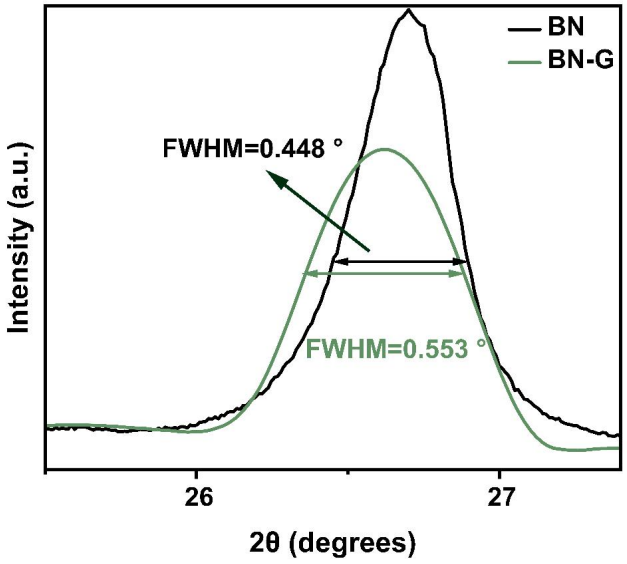

Supplementary Figure 2. Characterization of pristine BN and functionalized BN-G with a magnified view of the (002) diffraction peaks.

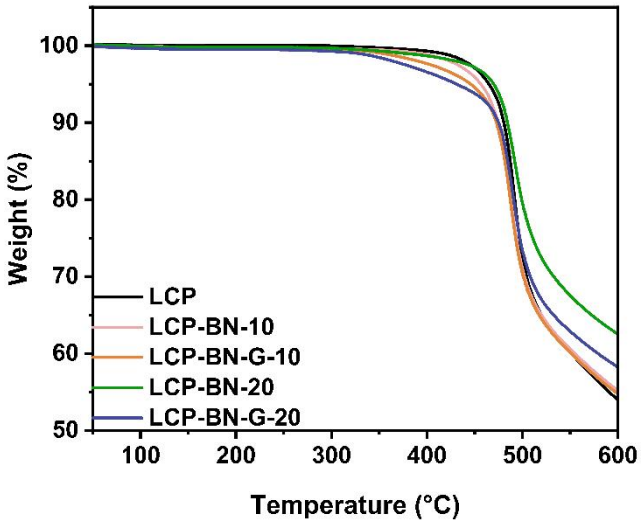

Supplementary Figure 3. TGA curves of LCP and its BN/BN-G composites.

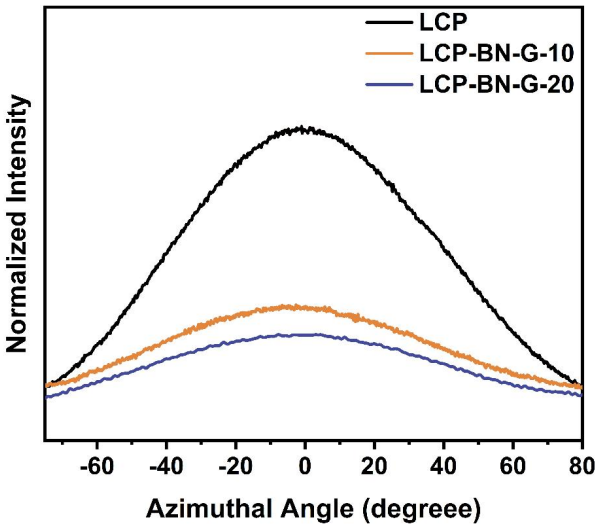

Supplementary Figure 4. Azimuthal intensity profiles of the LCP matrix at 2θ≈20°.

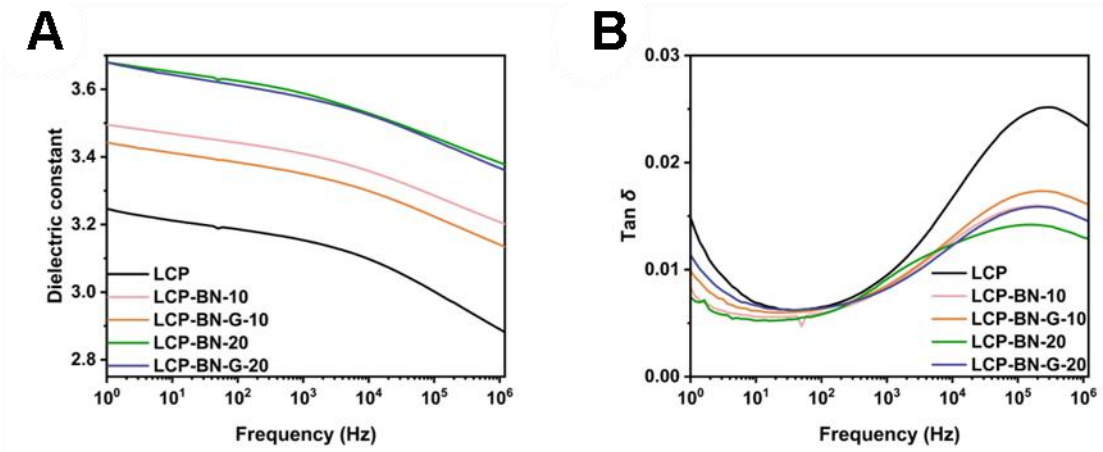

Supplementary Figure 5. Dielectric properties of LCP and its BN/BN-G composites. (A) dielectric constant and (B) dissipation factor.

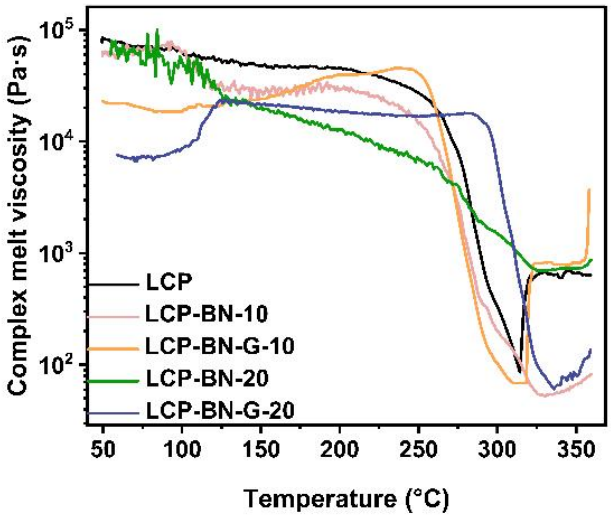

Supplementary Figure 6. Rheological behavior curves of LCP and its BN/BN-G composites.

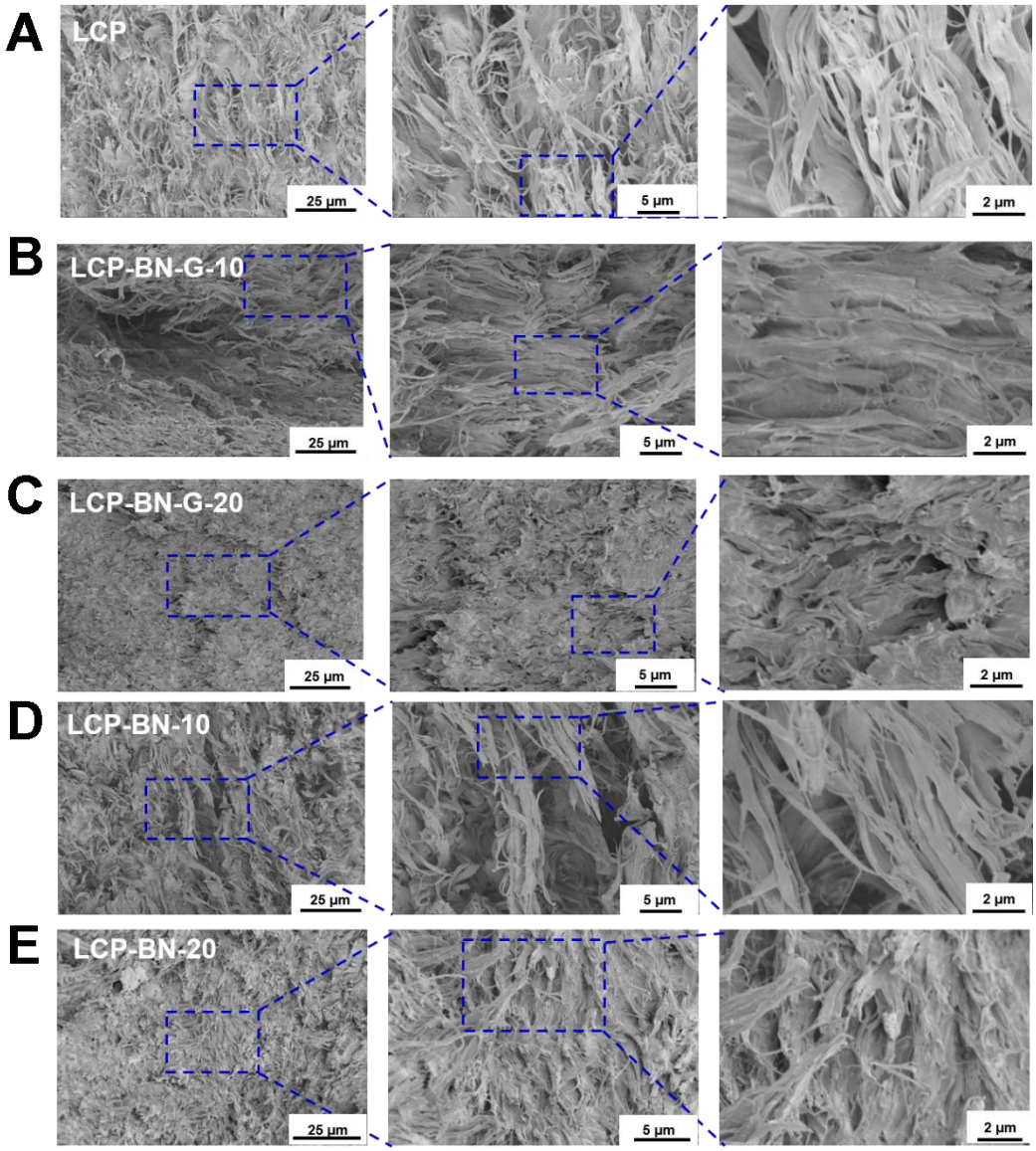

Supplementary Figure 7. Comparative SEM fracture surface morphologies of neat LCP, LCP-BN, and LCP-BN-G composites at different magnifications: (A) LCP, (B) LCP-BN-G-10, (C) LCP-BN-G-20, (D) LCP-BN-10, and (E) LCP-BN-20.

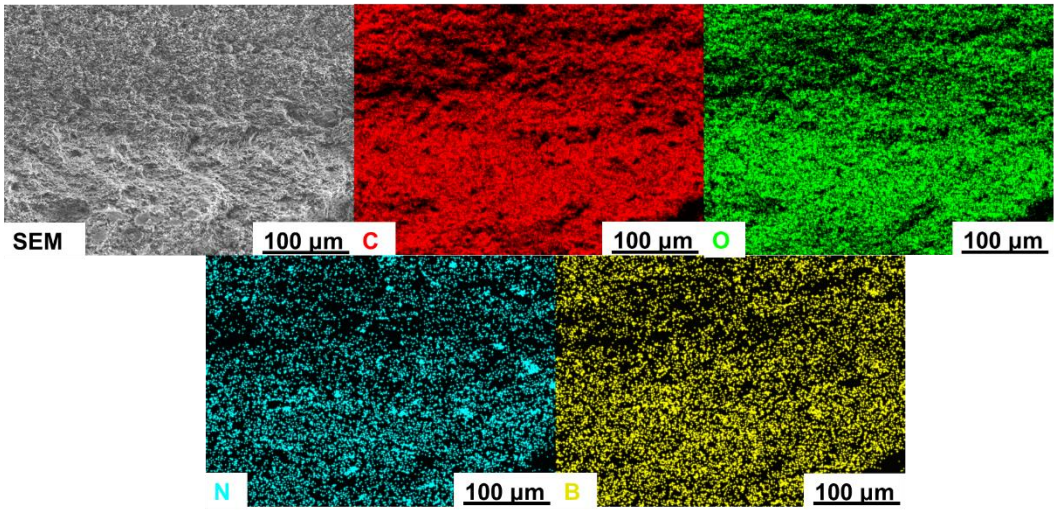

Supplementary Figure 8. The surface element distribution of the LCP-BN-G-20.

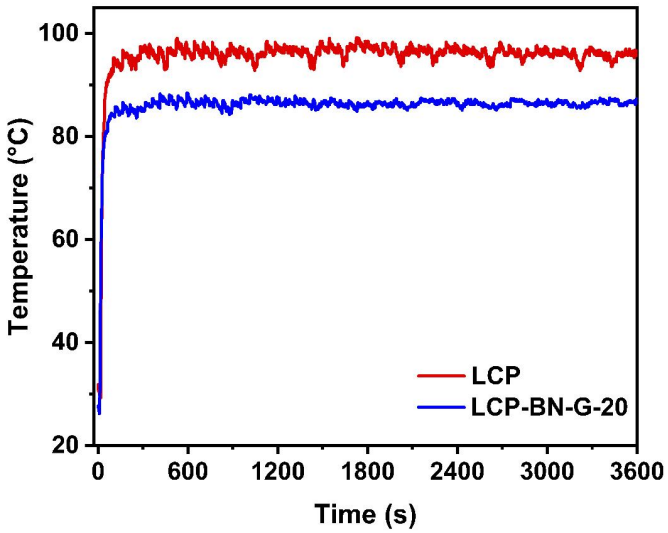

Supplementary Figure 9. Comparison of surface temperature variation between pure LCP and LCP-BN-G-20 substrates during 3600 s of continuous LED operation.

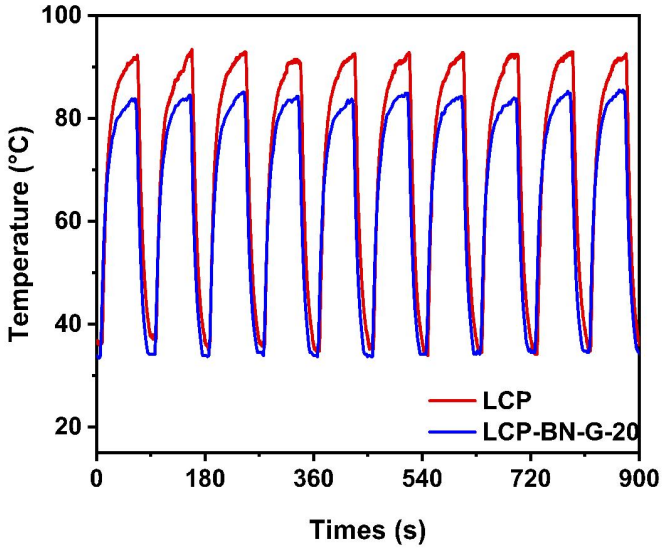

Supplementary Figure 10. Surface temperature variation of pure LCP and LCP-BN-G-20 substrates during ten cycles of 60 s heating and 30 s cooling.